Article:
Liberti, E, Menzel, R, Shaffer, MSP et al. (1 more author) (2016) Probing the size dependence on the optical modes of anatase nanoplatelets using STEM-EELS. Nanoscale, 8 (18). pp. 9727-9735. ISSN 2040-3364

https://doi.org/10.1039/C5NR09264G

Probing the size dependence on the optical modes of anatase nanoplatelets using STEM-EELS

Emanuela Liberti[1,‡,*], Robert Menzel[1,§], Milo S. P. Shaffer[1], David W. McComb[1,¶]

[1]Imperial College London, Department of Materials, London SW7 2AZ, UK

*Corresponding author: emanuela.liberti@materials.ox.ac.uk

Present Addresses

[‡]Department of Materials, University of Oxford, Parks Road, Oxford OX1 3PH, UK

[§]School of Chemistry, University of Leeds, Woodhouse Ln, Leeds LS2 9JT

[¶] Department of Materials Science & Engineering, The Ohio State University, Columbus, OH 43210, USA

†**Electronic supplementary information (ESI) available:** Histograms of length and thickness of the platelets; perpendicular component of dielectric function; thickness dependence of perpendicular component of loss function; VEEL spectra of edge-on platelet along c-axis; VEEL spectra of face-on and edge platelets stacks.

Abstract

Anatase titania nanoplatelets predominantly exposing {001} facets have been reported to have enhanced catalytically properties in comparison to bulk anatase. To understand their unusual behaviour, it is essential to fully characterize their electronic and optical properties at the nanometer scale. One way of accessing these fundamental properties is to study the dielectric function. Valence electron energy-loss spectroscopy (EELS) performed in the scanning transmission electron microscope (STEM) is the only analytical method that can probe the complex dielectric function with both high energy (< 100 meV) and high spatial (< 1 nm) resolution. By correlating experimental STEM-EELS data with simulations based on semi-classical dielectric theory, the dielectric response of thin (< 5 nm) anatase nanoplatelets was found to be largely dominated by characteristic (optical) surface modes, which are linked to surface plasmon modes of anatase. For platelets less than 10 nm thick, the frequency of these optical modes varies according to their thickness. This unique optical behaviour prompts the enhancement of light absorption in the ultraviolet regime. Finally, the effect of finite size on the dielectric signal is gradually lost by stacking consistently two or more platelets in a specific crystal orientation, and eventually suppressed for large stacks of platelets.

Table of Content (TOC) Figure

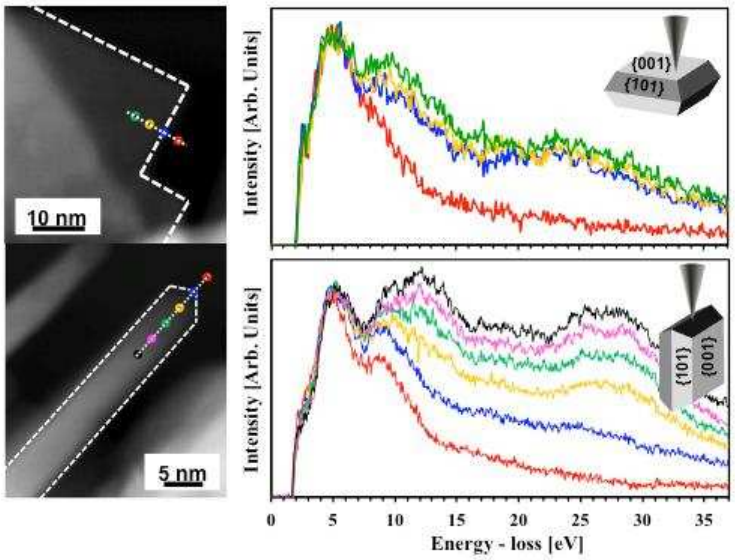

Local, size dependence of the optical modes of thin anatase nanoplatelets (< 5 nm) in response to an electron probe.

Introduction

Titanium dioxide (TiO_2) is a widely used photocatalyst of commercial importance,[1,2] and is exploited by the energy industry in a variety of applications, such as photovoltaics (e.g. dye-sensitized solar cells),[3] photochromics,[4] water-splitting devices[5] and purification of water and air.[6] Indeed, owing to its abundance, low cost, non-toxicity, and unique physical properties, TiO_2 represents one of the most favoured metal oxide photocatalyst.[7,8] Due to its large band gap (> 3 eV), TiO_2 is mostly active in the ultraviolet range. In order to enhance the photoresponse of titania numerous strategies, including nanostructuring have been employed.[9,10] To fully exploit the properties of titania nanostructures, understanding of the electronic structure and optical properties at the nanoscale is essential. One way of accessing these properties is to study the dielectric function. The dielectric behavior of solids originates from the collective, or direct, excitation of valence electrons, in response to an electromagnetic perturbation, such as photons or electrons.[11] The real and imaginary parts of the complex dielectric function provide the optical properties of the solid, which, in turn, correlate to its electronic properties. At the nanoscale, an established method to measure dielectric properties is valence electron energy-loss spectroscopy (VEELS).[12] When carried out in combination with high-resolution (scanning) transmission electron microscopy (STEM), VEELS provides information at the nanoscale, over an energy range that spans from the visible to the extreme ultra-violet (0-50 eV). Furthermore, with modern electron monochromators, the attainable energy resolution is < 0.1 eV, which is comparable to the resolution accessible by optical techniques that, in contrast, have limited spatial resolution. Numerous theoretical and experimental VEELS investigations of the dielectric function of bulk TiO_2 can be found in the literature.[13-16] On the other hand, the dielectric behavior of individual

TiO_2 nanostructures has been poorly investigated, mostly because conventional optical techniques lack atomic resolution. In a recent study,[17] Wang et al. used spatially resolved EELS (SREELS) to investigate the dielectric response of an individual multiwall $H_2Ti_3O_7$ nanotube. In contrast to the bulk case, a TiO_2 particle of diameter 100 nm, the main features of the EEL spectrum of the nanotube were found to be surface oscillating modes originating at the large surface area of the tube (< 8 nm), as well as due to the coupling of the walls. Despite the importance of such findings, no detailed interpretation of the size effects has been reported in relation to anatase nanostructures of confined thickness, including two-dimensional nanosheets. At the nanoscale, anatase is the most stable, catalytically active phase of TiO_2. Owing to the high density of active sites associated with under-coordinated Ti and O atoms, the {001} crystal facet of anatase is theoretically considered the most reactive and selective surface of anatase.[18] Among two-dimensional anisotropic anatase nanostructures, TiO_2 nanoplatelets with exposed {001} facets have been theoretically and experimentally shown to exhibit superior performances in many photocatalytic applications,[19-21] including plasmon enhanced photocatalysis.[22-24] Despite the intensive research on the controlled synthesis of the platelets, electronic and optical characterization are still missing at the nanoscale. This study reports experimental VEELS data of individual anatase nanoplatelets with {001} facets, and, in this way, presents a detailed study of the size effect on the dielectric response of anatase. The data provide a basis for measuring the complex dielectric function as a function of sample thickness. The dielectric function can be used to determine useful optical properties of individual anatase nanoparticles, such as their refractive index and optical absorption coefficient, which are of interest to a large range of disciplines, including photocatalysis and optics. In this work, the effect of finite crystal thickness is investigated in two cases. In the first case, the VEEL spectra are collected for platelets aligned in two crystallographic orientations, where the electron probe

penetrates a crystal thickness of < 5 nm and > 20 nm, respectively. Similarly, in the second case, stacking of two or more platelets is exploited to examine changes in the spectral features. Furthermore, the spectra were recorded under both penetrating and non-penetrating (aloof) configurations, to distinguish between surface and volume excitations. In all these cases, the experimental results, including coupling effects between distinct platelets, are interpreted by VEELS calculations based on semi-classical dielectric theory.[25]

Results and Discussion

Valence electron energy-loss spectra were successfully obtained from individual cleaned anatase platelets (Figure 1a). In the annular dark-field (ADF) STEM image shown in Figure 1b, an individual platelet is outlined with dashed lines. As ADF images exhibit stronger contrast in thicker areas, only the top left region, above the bright diagonal line, is assumed to be a single platelet. Previous TEM studies have shown that individual anatase platelets have the shape of a truncated octahedron, which, in a face-on configuration, preferentially orients along a [001] orientation.[26] Assuming this zone axis, in Figure 1b, the probe is equidistant from the {010} edges of the platelet, along the line of pixels marked by open circles. Each EEL spectrum is labeled according to the distance of the probe, x, from a {100} edge, where $x = 0$. This distance is positive in vacuum (aloof geometry)[12] or negative in transmission. In the aloof, non-penetrating geometry, two main peaks are observed around 5 eV and 8 eV, respectively. The peak at 8 eV gradually blue shifts as the probe approaches the interface. Inside the specimen, at $x = -12$ nm from the edge, the main peaks are located at 4.7 eV and 9.4 eV. Furthermore, as the probe penetrates the platelet the peak at 9.4 eV broadens with a shoulder at 12 eV and a broad peak starts to appear between 16 eV and 30 eV.

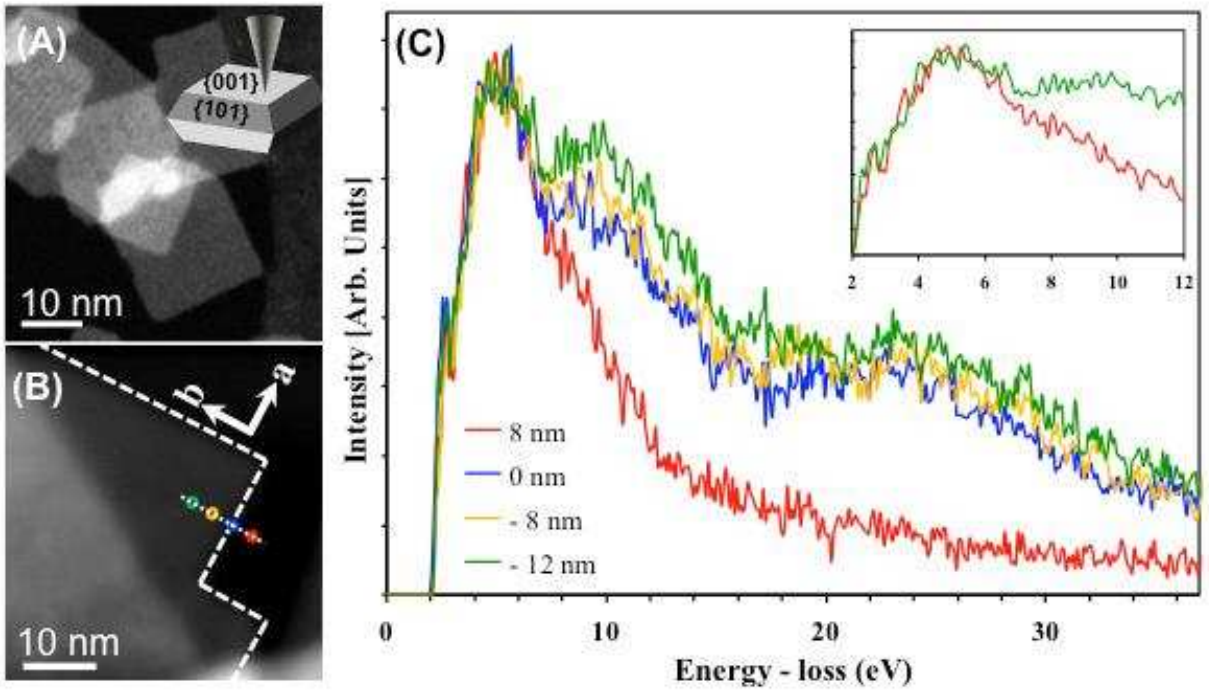

Figure 1. Annular dark-field image of anatase nanoplatelets (a) with {001} exposed facets. Valence electron energy-loss spectra acquired from a single platelet, shown in (b), are plotted in (c), as a function of probe position (open circles in (b)). Dashed lines in (b) outline the platelet facets. Open circles in (b) indicate the probe position at each pixel. Probe distances from a {100} edge of the platelet are positive in vacuum, or negative, in transmission. In (c), the inset illustrates an enlarged view of the first and last spectrum, in the 2 – 12 eV energy range. The spectra were acquired with an energy resolution of 0.7 eV, a collection semi-angle of 11 mrad, an energy dispersion of 0.1 eV/pixel, and a dwell time of 0.2 s.

To help identify the origin of the features in the EEL spectra of the platelet, a comparison with the bulk case is required. For this comparison, the energy-loss function of bulk anatase, as well as the real and imaginary parts of the dielectric function, $\varepsilon_1(E)$ and $\varepsilon_2(E)$ were measured using STEM-EELS (Figure 2). The single-scattering distribution, S(E), which is proportional to the energy-loss function, was obtained after deconvolution of the multiple scattering from the EELS spectrum of

an anatase substrate, oriented in the [001] and [100] zone axes. In the first case, the electron beam is parallel to the anisotropic c-axis, and the dielectric tensor corresponds to the component $\varepsilon_{\perp}$ (ε_{xx} , ε_{yy}) associated with the response for a momentum transfer perpendicular to the c-axis. In the latter case, the electron beam is perpendicular to the c-axis, however in this geometry the dielectric tensor is a combination of $\varepsilon_{\perp}$ and $\varepsilon_{\parallel}$ (ε_{zz}) (see Figure S1a). The real and imaginary parts of the dielectric function were obtained from the single-scattering distribution S(E) by performing the Kramers-Kronig transformations, after removing the effect of the relativistic Čerenkov losses using the off-line correction algorithm proposed by Stöger-Pollach (see Figure S1b).[27] These experimental data provide substantive agreement with the dielectric function of anatase measured by reflectance spectrometry.[14] For clarity's sake, only the component of the dielectric function obtained from the [100] substrate is shown in Figure 2 (see Figure S1a for the $\varepsilon_{\perp}$ component). Due to the low angular resolution used in STEM-EELS, where the spectrum is averaged over a large range of scattering vectors due to the large collection angle, the effect of crystal anisotropy on the loss spectrum is small below 30 eV (inset in Figure 2). At large collection angles, the anisotropic behavior of anatase mostly affects the energy position and intensity of the interband transitions, as well as that of the volume plasmon peak. Further study of the bulk case is beyond the scope of this work and will be published elsewhere.

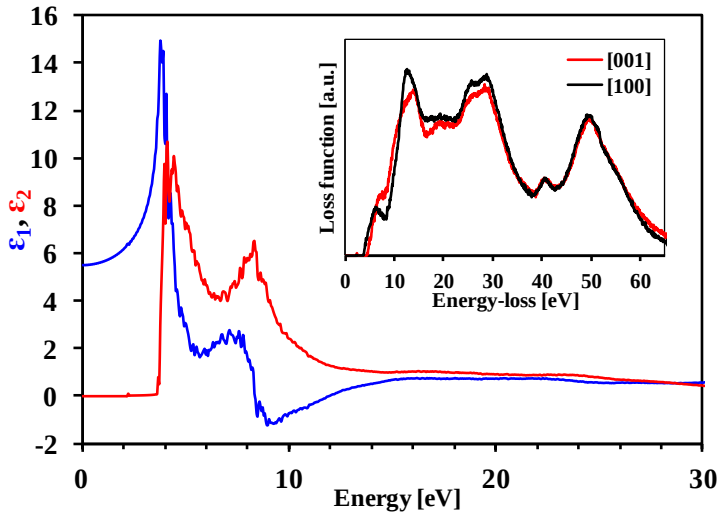

Figure 2. Component of the dielectric function of bulk anatase, obtained from a [100] substrate, separated into the real, ε_1, and imaginary part, ε_2, in the blue and red curves, respectively. The inset shows the energy-loss function, S(E), obtained from the deconvolution of the experimental energy-loss spectrum, for both [100] (black) and [001] (red) components. The dielectric functions were retrieved from S(E), after removal of the Čerenkov losses using the Kramers-Kronig transformations.

By examining the dielectric function of bulk anatase according to the dielectric theory,[25] all the features in S(E) can be identified. At the energy where $\varepsilon_1(E)$ crosses the abscissa with positive slope (Figure 2), a volume plasmon is excited in the specimen, resulting in a maximum at 12.5 eV in the energy-loss spectrum. Similarly, a volume excitation is observed in the loss spectrum at 28 eV, corresponding to a linear increase of $\varepsilon_1(E)$ starting at around 25 eV, and a linear decrease of $\varepsilon_2(E)$ at around the same energy. This discrepancy between energies arises from the damping of the plasmon excitation which is to be expected in an insulating material.[12] Additional peaks in the energy-loss function of anatase can be attributed to interband transitions from valence to conduction bands that occur at the energy of the maxima in $\varepsilon_2(E)$. At low energy-loss, the peak

maxima at 4.5 eV and 8 eV in $\varepsilon_2(E)$ correspond to single electron transitions from the O 2p orbitals in the valence band to the Ti 3d t_{2g} and e_g orbitals in the conduction band, which result in the 3 – 8 eV peak in the energy-loss function, after the band gap onset.[14-16] In order to correlate the bulk features of the loss function of anatase with those of the platelet, the dielectric functions in Figure 2 were used to perform EELS calculations using the relativistic expression of the inelastic scattering probability formulated by Kröger.[27, 28] At normal incidence, the platelets can be regarded as thin foils of anatase. For this geometry, the inelastic scattering probability calculated by the Kröger equation predicts both bulk and surface losses, whose frequency and intensity vary according to the thickness of the slab. To identify surface excitations in a thin slab of anatase, it is useful to calculate their angular dispersion by solving the relativistic Kröger equation as a function of energy-loss and scattering angle, θ. Figure 3 shows the simulated E-θ maps for 50 nm, and 5 nm thick anatase slabs. In the 5 nm slab, two main features have a strong dispersive character, which tend asymptotically to two energy-loss values at 5 eV and 9.6 eV, respectively. These features can be identified as surface excitations of anatase. Indeed, for the 50 nm slab, the angular dispersion of the surface features is negligible and their excitation is suppressed. Furthermore, as the slab becomes thicker, bulk related features start to appear, such as surface guided modes, at discrete energy-losses below 4.1 eV, where $\varepsilon_1 > \varepsilon_2$. This condition is, in fact, required for the existence of the surface guided modes.[29] For thicknesses larger than 50 nm, the guided modes couple with the Čerenkov radiation (not shown).

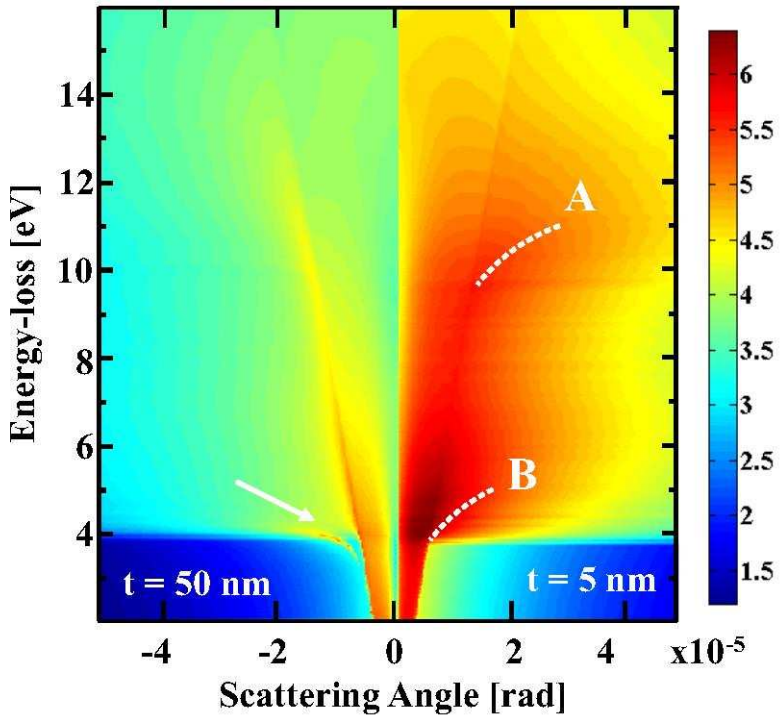

Figure 3. Simulated E-θ maps (E is the energy-loss and θ is the scattering angle) for two anatase slabs of thicknesses 50 nm and 5 nm, showing the angular dependence of the energy-loss spectrum. The dashed lines A and B indicate the dispersion of the surface modes. Close to the light line, the arrow points at the guided light modes.

Analyzing in more detail the surface excitations of a thin anatase slab, the asymptotic value of 9.6 eV represents the energy of the planar surface plasmon mode (SP), for which the condition $\varepsilon_1 = -1$, required for the excitation of a non-radiative surface plasmon, is satisfied.[12] Although the dispersive character of the feature at 5 eV indicates that it is surface related, its origin cannot be readily interpreted on the basis of the dielectric theory. At the energy-loss of 5 eV, in the energy-loss spectrum, an interband transition occurs (peaks in the loss function are generally found at higher energy losses than in ε_2).[12] According to recent findings, surface features that are excited at energies near to interband transitions may be associated to a particular type of surface excitations

named surface exciton polaritons (SEPs).[30-33] SEPs are collective excitations of delocalized Wannier-type excitons originating at the surface of materials. The existence of a surface exciton polariton requires that $\varepsilon_2 > |\varepsilon_1| > 0$, a condition[30] satisfied by many semiconductors and insulators above the band gap, including anatase. In addition to this condition, the thickness of the sample must be small enough to allow the imaginary part, k_i, of the complex wavevector k to be negligible, a condition that is also satisfied for a thin platelet.[30] There have been limited investigation of SEPs using EELS, and they have only recently observed in semiconducting nanostructures, such as HfO_2 thin films,[30] GaN nanoprisms,[31] and ZnO nanorods[32, 33] in aloof geometry where the interband transitions are suppressed and the corresponding surface features enhanced.

Having established two of the main surface excitations of an anatase slab from their angular dispersion, it is useful to analyze their behavior with thickness. Figure 4 shows the results of calculations of the EEL spectra of anatase slabs of increasing thickness, integrated over the spectrometer collection angle. For the sake of simplicity, only the component of the loss function corresponding to Figure 2 is shown in Figure 4 (see Figure S2a for the alternative component).

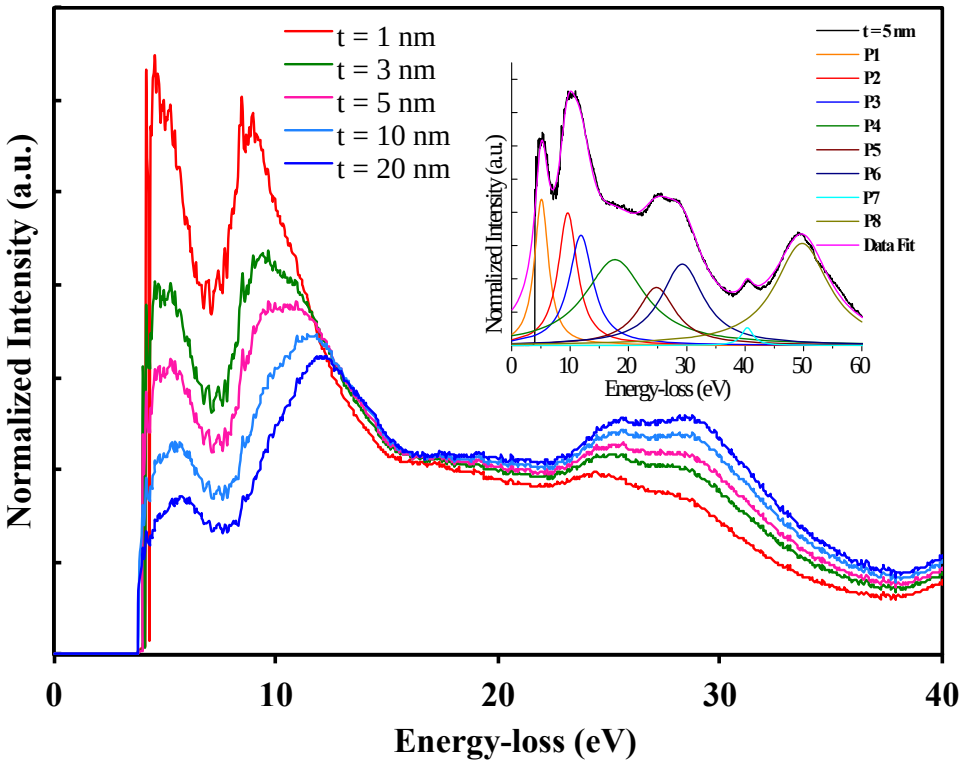

Figure 4. Simulated relativistic inelastic scattering probability of 300 keV electrons penetrating at normal incidence a thin film of anatase of different thicknesses (t). The EELS probability was calculated from the dielectric functions in Figure 2 and integrated over a collection semi-angle of 11 mrad. The spectra were normalized by their integrals. Characteristic peaks, which have been identified with electronic transitions of anatase, are labeled as P1-P8 in the inset, where the scattering probability for t = 5 nm was fitted with Lorentzian peaks. Peaks P7 and P8 are the $M_{2,5}$ edges of Ti.

The main surface and volume features of the spectra can be assigned as follows. The volume plasmon peak of anatase, labeled as P3, is located at 12.5 eV. The corresponding surface plasmon mode is labeled as P2. The intensity of this mode, relative to that of the volume plasmon, is enhanced for thinner slabs, an event known as the Begrenzungs (boundary) effect.[12] The resonance

energy of the SP mode gradually blue shifts with thickness, and eventually reaches the asymptotic value of 9.6 eV in a 10 nm thick slab. This blue shift can be explained in terms of coupling of the surface modes, which occurs in very thin slabs.[28, 34, 35] In the dielectric formalism, the surface plasmons at the top and bottom surfaces of a thin slab can overlap and couple, resulting in the splitting of two plasmon modes. Higher energy modes have an antisymmetric distribution of charge at opposite surfaces the surfaces of the slab, while low energy modes are symmetric. As the thickness of the slab reduces, the energy of the symmetric modes shifts towards lower energy-losses, while the energy of the antisymmetric modes shifts towards higher energy-losses, resulting in a larger splitting. Due to the large integrated momentum transferred of a STEM-EELS experiment, the energy-loss probability of the antisymmetric modes vanishes rapidly, thus typically only the symmetric plasmon modes are measured.[36, 37] Hence, the blue shift of peak P2 with thickness is due to the coupling of the symmetric plasmon mode. This coupling only occurs for slab thicknesses smaller than 10 nm. This distance is consistent with the value of thickness v/w_p = 12 nm, within which the transmitted 300 keV electrons, of velocity *v,* excite surface rather than bulk plasmons.[12,38] For slabs thicker than 10 nm, peak P2 is suppressed. At low energy-loss, the spectrum of a thin slab of anatase is dominated by peak P1, located at around 5 eV. The intensity of this peak, relative to that of the bulk plasmon, is rapidly reduced with increasing thickness. As the energy of P1 is located in the proximity of an interband transition, it is possibly linked to the existence of a SEP. As consequence of this surface effect, the position of the interband transition shifts towards higher energy losses with increasing thickness. For t > 10 nm, P1 is not affected by the surface loss. The remaining peaks of the loss spectrum labeled as P4, P5, P6 are mostly bulk features. Peak P4 is a broad excitation that extends over the energy range of 15 eV to 20 eV, for all the thicknesses investigated. This spectral feature corresponds to a peak in ε_2 at 17

eV, identifying a broad interband transition. The intensity of P4, related to that of the surface losses, grows with thickness suggesting its bulk character. Peak P5 is also an interband transition, related to the maximum of ε_2 at 23 eV. It occurs at 25 eV for all thicknesses investigated, and, similarly to P4, it is a volume feature. Finally, as pointed out by the bulk study, peak P6 is also a volume collective excitation.

To summarize, as the slab becomes thinner, surface-like excitations start to dominate over volume excitations. In this case, the spectral features of the energy-loss spectrum are mainly attributed to the imaginary part of the dielectric function, as the real part of ε is mostly related to volume excitations.[38-40] For this reason, the shape of the EEL spectrum of a thin slab resembles that of ε_2.

The calculated energy-loss spectrum of a 5 nm thick slab of anatase, match closely the simulated data obtained for the face-on platelet in Figure S2b. By comparison, the peaks at 4.7 eV and 9.4 eV can be assigned to the P1 interband transition of anatase and the P2 surface plasmon mode. In contrast to the case of bulk anatase, P1 is the most intense peak of the spectrum, as the interband transition at 4.7 eV is enhanced by the SEP. The broad shoulder following P2 is the volume plasmon peak P3. This volume excitation is considerably less intense than in the bulk case, due to the confined thickness of the platelet. The broad excitation at 16-35 eV is also a volume related feature, given by the convolution of the P4, P5 interband transitions of anatase and the P6 collective excitation (see Figure S2b). The energy of the peaks in transmission does not change with probe position for distances larger than 5 nm from the edge of the platelet. In aloof geometry, when the probe does not penetrate the platelet, the volume features are suppressed and only the surface excitations contribute to the EEL spectrum. To interpret the nature of this surface peaks further dielectric calculations are required to account for the sample geometry at glancing incidence.

However, recent investigations of flat nanoprisms[31,41,42] suggest that surface plasmons are excited at the edge and corners. Thus, for the nanoplatelets, it is likely that only the edge mode is excited at the vacuum interface. This edge mode is associated with a symmetrical charge distribution between the top and bottom surfaces, as for the surface plasmon in transmission. Hence, the peak at 8 eV in the aloof spectrum might be associated with the edge mode of the platelet, while the peak at 4.7 eV could be identified as the delocalized surface plasmon polariton.

In the platelet specimen, the nanocrystals are mostly oriented along two zones axes, namely [001] and [100].[26] Platelets oriented in the [100] zone axis are referred to as 'edge-on'. In contrast to the case of a face-on platelet, the effect of thickness in the edge-on configuration plays a double role in the determination of the features of the EEL spectrum. To explain these effects in more detail, the case of an edge-on platelet is examined in Figure 5.

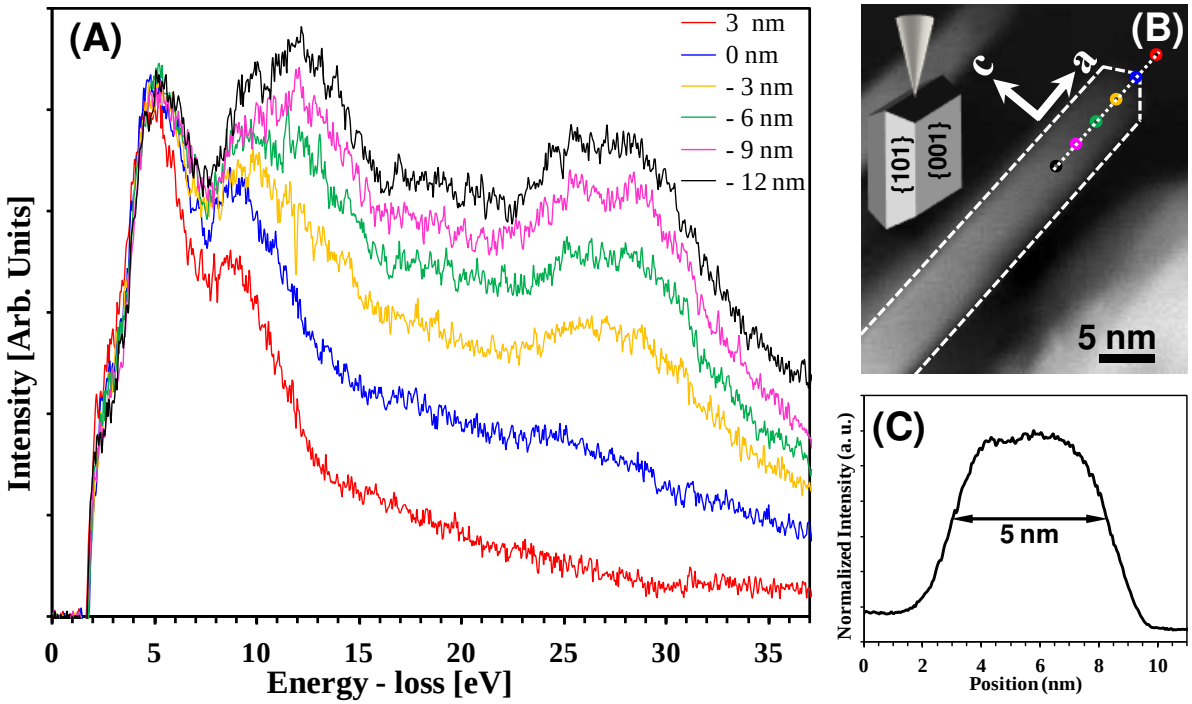

Figure 5. Valence electron energy-loss spectra (a) acquired from the edge-on anatase platelet marked in the ADF image in (b) by dashed lines. The spectra were taken at the probe

positions indicated by the open circles in (b). The distance of the probe from the tip of the platelet is positive when in vacuum, or negative, in transmission. The thickness (along the c-axis) of the platelet is taken as the full width at half maximum of the intensity profile at the last spectrum position as shown in (c). The spectra were acquired with an energy resolution of 0.7 eV, a collection semi-angle of 11 mrad, an energy dispersion of 0.05 eV/pixel, and a dwell time of 0.3 s.

When the probe is scanned parallel to the interfaces at normal incidence, at x = -12 nm, except for the 9.6 eV peak, all other features of the EEL spectra are found in the energy-loss function of bulk anatase. This resemblance is due to the crystal thickness along the beam direction, which is several tens of nanometers, comparable to that of a thick anatase slab. On the other hand, perpendicularly to the beam direction, the crystal thickness is considerably smaller (t = 5 nm), and the probe is confined within a small distance between the interfaces. When the distance of the electron probe is below 5 nm, the plasmon mode is enhanced at 9.6 eV with respect to the main bulk plasmon. Furthermore, at low energy-loss, the P1 interband transition is more intense than in the bulk case, due to the surface effect. In contrast to the transmission case, the EEL spectra in the aloof geometry are similar to those obtained for face-on platelets. The similarity is explained by considering the two-dimensional geometry of the near-field experiment. In both face-on and edge-on cases, the electron trajectory is either parallel or perpendicular to the smallest distance between the interfaces,[38] thus the response of the surfaces is indeed alike in the two cases. It is also worth noting that in the transmission geometry identical features to the case examined in Figure 5 are also observed in the EEL signal for electron trajectories approaching the center of the platelet along the c-axis (Figure S3).

When platelets are aligned along similar orientations, they are often found overlapping one another. This overlap can be exploited to investigate changes of the low loss spectrum upon interaction of the electron beam with a stack of platelets. Figure 6 shows the overlap between two anatase edge-on platelets along the c-axis. In the ADF image, dashed lines outline the platelets stack, while the interface between the platelets is left unmarked. The thickness of the platelets along the c-axis is 7 nm and 6 nm for the left and right case, respectively, as indicated by the intensity profile in Figure 6c. Provided that the acquisition parameters used in the experiments are identical, the spectra obtained for the overlapping platelets can be compared to those of a 6 nm thick, isolated platelet (Figure S3), in the same probing geometry. In aloof mode, the peak energies of the surface plasmons in the overlapping case are blue shifted with respect to the isolated case. As discussed earlier, the blue shift of the surface plasmons in a thin slab is caused by an increment of slab thickness. In the transmission geometry, the plasmon energy at 9.6 eV, observed for the isolated slab, is not directly visible in the overlapping case.

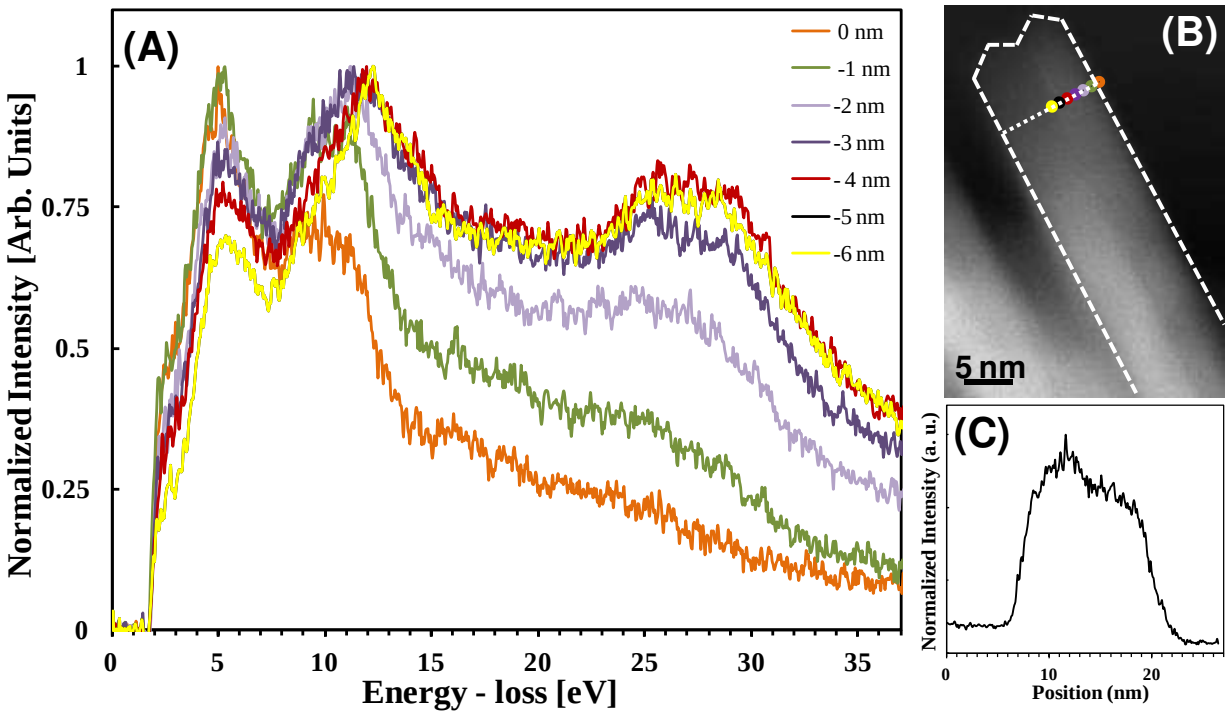

Figure 6. Valence electron energy-loss spectra (a) acquired from the platelet stack marked in the ADF image by dashed lines (b). The spectra were taken at the probe positions indicated by the open circles in (b). The probe distance from the interface with vacuum is negative within the stack. The intensity profile along the line of probe positions is also shown in (c). The spectra were acquired with an energy resolution of 0.7 eV a collection semi-angle of 11 mrad and an energy dispersion of 0.05 eV/pixel, and a dwell time of 2 s.

According to the calculations in Figure 3, the fact that no strong surface plasmon is observed indicates that the overall thickness interacting with the electron beam is larger than 10 nm. Thus, if the overall stack of platelets is considered in the interaction, the EEL signal is the response of a 14 nm thick slab of anatase. At the interface with vacuum, the surface (interface) plasmon mode of the slab is excited at 9.6 eV, however at 5 nm from the interface this peak is suppressed by the volume plasmon. Similarly, as the probe moves away from the interface, the volume excitations gradually dominate, and eventually replace the surface features at low energy-loss. To summarize,

when the overlap between edge-on platelets occurs, the EEL signal is the result of the interaction of the electron beam with the full stack of platelets. This aspect suggests that the overlapping platelets act as one block of material, the thickness of which determines the shape of the spectrum. Thus, eventually, by increasing the number of platelets up to a certain number, the platelet stack will replicate the case of a semi-infinite plane of anatase (Figure S4). In order to understand whether there exists any epitaxial relationship or any orientational order between platelets of a stack acting as a single block of anatase, the analytical formulation of the scattering probability used until now to calculate the EEL spectrum of the platelets is no longer suitable. To replicate the stack geometry, a suitable starting model would consist in a multilayered slab of anatase, with a dielectric layer interposed between the slabs. However, this refined geometry requires a numerical formulation of the scattering probability,[43, 44] rather than an analytical one, which is computationally expensive, and goes beyond the scope of this work. To further investigate the effect of platelet stacking, the experiments were replicated for the case of two or more overlapping face-on platelets. Face-on nanoplatelets align along the [001] zone axis, however alternative orientations are also found in proximity of the [111] zone axis.[45] In the latter case, the projected two-dimensional shape of the platelets is rhombohedral, while in the former case the platelet projection is typically a square. An example of overlapping platelets aligned along the [111] zone axis is shown in the ADF image of Figure 7.

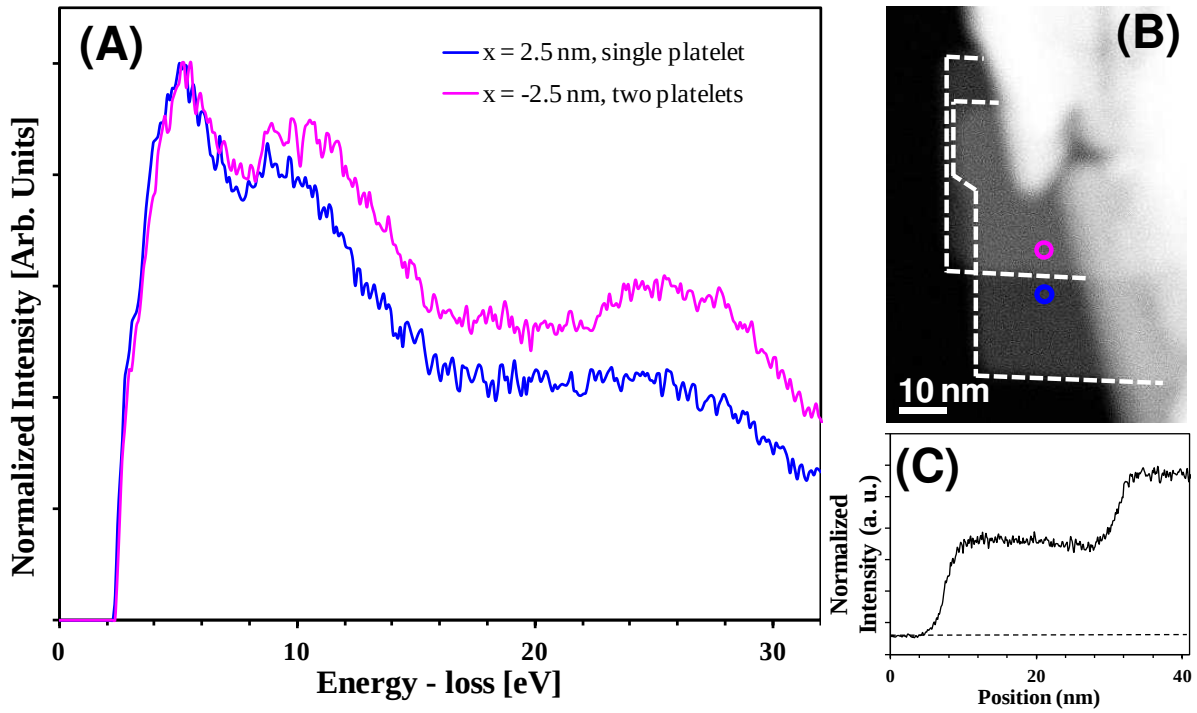

Figure 7. Valence electron energy-loss spectra (a) acquired from the platelet stack in the ADF image in (b). Each platelet is marked by dashed lines. The spectra were taken at the probe positions indicated by the open circles in (b). The intensity profile along the line of probe positions is shown in (c). The spectra were acquired with an energy resolution of 0.7 eV, a collection semi-angle of 4.5 mrad, an energy dispersion of 0.05 eV/pixel, and a dwell time of 1 s/pixel.

The overlap region is characterized by an increase of the image intensity due to the increment of the crystal thickness given by the stacking. The intensity increase in this region is approximately double the intensity of the single platelet. The EEL spectrum of the platelet stack is plotted in Figure 7 against that of one platelet. The spectral features observed previously for a thin slab of anatase about 5 nm thick, in transmission, are replicated in the spectrum of the individual platelet. Furthermore, similarly to the stacking of edge-on platelets, in the overlap region the volume features above 10 eV are enhanced due to the increment of the slab thickness along the beam

direction. The result can be replicated for the case of three overlapping platelets of mixed morphologies (Figure S5). For the stacking of three platelets, only bulk features contribute to the EELS spectrum in transmission.

Conclusions

In conclusion, this study provides dielectric data of thin anatase platelets with exposed {001} facets, obtained using valence electron energy-loss spectroscopy. In addition to investigating the optical modes of thin platelets, the results also document the size effect on the dielectric response of anatase. To interpret the experimental data, EELS spectra in transmission were simulated analytically using the full relativistic expression of the Kröger equation, as a function of thickness and scattering angle. On the basis of these calculations, the two dominating features of the EEL spectrum of individual platelets were found to be an interband transitions around 5 eV enhanced by the surface exciton polariton and the surface plasmon mode at around 9.6 eV. For platelets less than 10 nm thick, these characteristic modes are greatly enhanced in comparison to the bulk case and the dielectric function is largely determined by its absorptive imaginary part. In the context of photocatalysis, the imaginary part of the dielectric function is of particular interest, representing the optical absorption spectrum. The electron energy-loss data presented in this work clearly show that by forming nanoplatelets of reduced thickness it should be possible to improve the photocatalytic activity of anatase in the ultraviolet regime. While improve improved catalytic activity of thin anatase platelets has been experimentally observed, this effect is usually exclusive attributed to the unusual surface chemistry of the exposed (001) crystal facets. Our findings clearly show that surface plasmon effects are an important additional factor that needs to be taken in account. Furthermore, the data show that the frequency of the optical modes can be tuned

according to the platelets thickness. This tunable effect can, for example, be obtained by assembling two or more platelets along one specific crystallographic orientation. This size effect also implies that complete individualization of the platelets is needed in order to exploit their optical behaviour in optical and photocatalytic applications, as stacks of even only two platelets can result in the typical dielectric response of bulk anatase. Finally, the results have direct relevance to the study of the enhanced photocatalytic properties in TiO_2/metal nanoparticle heterostructures. In these systems, the metal nanoparticles enhance photocatalytic activity through a range of effects, including sensitization (extending optical absorption into the visible range of the electromagnetic spectrum), electron-trapping (suppressing electron-hole recombination), and plasmonic enhancement (promoting electron-hole formation in TiO_2 in the electric near-field of plasmon-excited metal nanoparticles). In this context, the qualitative and quantitative understanding of plasmonic effects and optical mode enhancement in individual anatase nanoparticles, as studied here, will provide a valuable tool for future experimental and theoretical studies of these complex systems.

Methods

Anatase nanoplatelets were synthesized via a hydrolytic reaction of titanium (IV) isopropoxide $Ti(O^iPr)_4$ in aqueous hydrofluoric acid, following the procedure described previously.[26] In the same study, the samples were characterized using X-ray diffraction (XRD), energy-dispersive X-ray spectroscopy (EDX) and electron diffraction (ED). The size distribution of the platelets was characterized by means of intensity profiles extracted from bright-field TEM images (see Figure S4 and S5 for histogram plots of length and thickness distribution). Typically, the platelets exhibit

a mean thickness of 4.5 ± 0.1 nm, while their mean edge length is found to be 50.1 ± 2.0 nm. The standard deviations of the distributions are 0.7 nm and 17.8 nm, respectively.

To avoid contamination build-up during EELS experiments, the as-received products were washed to remove any residual structure directing agent (SDA) from the surface. The platelets, 20 mg, were dispersed in 10 ml of 1 mM NaOH aqueous solution by bath sonication for 15 min, left stirring for 16 h, and subsequently centrifuged at 17000g for 30 min. Washing steps were repeated until a pH of 6 was reached. The washing treatment with dilute NaOH ensures the removal of isopropyl and fluorine surface groups, and the complete hydroxylation of the particle surfaces, which facilitates the breakup of large aggregates and enables electrostatic nanoparticle stabilization. Finally, the samples were drop-cast onto a 300 mesh carbon-coated Cu TEM Agar grid and left to dry overnight in air. Prior to the insertion into the electron microscope, the samples were plasma cleaned for 30 s,[46] using a Gatan Solarus 950 Advanced Plasma System with a hydrogen/oxygen mixed plasma at a flowing rate of 6.4 and 27.5 sccm for O_2 and H_2, respectively. The electron energy-loss spectra were acquired in an FEI Titan 80 – 300 kV microscope equipped with a monochromator, operating in STEM mode at 300 kV and extraction voltage of 4.5 kV. Typical energy resolutions during non-monochromated experiments were of 0.7 eV. Typically used probe sizes were of 0.5 nm and 0.3 nm in monochromated and non-monochromated experiments, respectively. The probe convergence semi-angle was of 10 mrad in all experiments. Additional acquisition parameters, such as collection angle, energy dispersion and acquisition time, are detailed for each experiment reported in the paper. The spectrum imaging (SI) technique, with sub-pixel scanning, was used to acquire an EELS data set. Spatial drift correction was performed during acquisition every 1, 5 or 10 pixels according to specimen drift. The EELS spectra were collected using a Gatan Tridiem 865 EEL spectrometer, and were corrected for the dark

current and gain variation of the photodiode during acquisition. To avoid background contribution from the amorphous carbon, the data were acquired for platelets overhanging a hole in the carbon support. The high-angle annular dark field (HAAF) survey images were acquired in STEM mode, using a convergence and collection semi-angle of 10 mrad, and 25–145 mrad, respectively. The EELS spectra were deconvoluted by the zero-loss peak and multiple scattering using the Fourier-log deconvolution routine available in the DigitalMicrograph software. The mirrored tail fitting model was selected in the routine, choosing a cut-off point of 1.5 FWHM.

Acknowledgment

The authors would like to acknowledge EPSRC EP/C51596X/1 and EP/G007314/1 grants that provided the financial support for this study.

References

(1) U. Diebold, *Surf. Sci. Rep.*, 2003, **46**, 53.

(2) A. L. Linsebigler, G. Lu and J. T. Yates Jr., *Chem. Rev.*, 1995, **95**, 735.

(3) B. O'Regan and M. Grätzel, *Nature*, 1991, **353**, 737.

(4) Y. Ohko, T. Tatsuma, T. Fujii, K. Naoi, C. Niwa, Y. Kubota and A. Fujishima, *Nature Mat.*, 2009, **2**, 29.

(5) M. Ni, M. K. H. Leung, D. Y. C. Leung and K. Sumathy, *Renewable Sustainable Energy Rev.*, 2007, **11**, 401.

(6) S. Dong, J. Feng, M. Fan, Y. Pi, L. Hu, X. Han, M. Liu, J. Sun and J. Sun, *RCS Adv.*, 2015, **5**, 14610.

(7) Y. Ma, X. Wang, Y. Jia, X. Chen, H. Han and C. Li, *Chem. Rev.*, 2014, **114**, 9987.

(8) J. Schneider, M. Matsuoka, M. Takeuchi, J. Zhang, Y. Horiuchi, M. Anpo and D. W. Bahnemann, *Chem. Rev.*, 2014, **114**, 9919.

(9) X. Chen and S. S. Mao, *Chem. Rev.*, 2007, **107**, 2891.

(10) M. Kapilashrami, Y. Zhang; Y. -S. Liu, A. Hagfeldt and J. Guo, *Chem. Rev.*, 2014, **114**, 9662.

(11) M. Fox, *Optical Properties of Solids*, Oxford University Press, Oxford, 2001.

(12) R. F. Egerton, *Electron Energy-Loss Spectroscopy in the Electron Microscope*, Springer, New York, 3rd edn., 2011.

(13) M. Launay, F. Boucher and P. Moreau, *Phys. Rev. B*, 2004, **69**, 035101.

(14) N. Hosaka, T. Sekiya, C. Satoko and S. Kurita, *J. Phys. Soc. Jpn.*, 1997, **66**, 877.

(15) R. Asahi, Y. Taga, W. Mannstadt and A. Freeman, *Phys. Rev. B*, 2000, **61**, 7459.

(16) S. -D. Mo and W. Y. Ching, *Phys. Rev. B*, 1995, **51**, 13023.

(17) J. Wang, Q. Li, L. -M. Peng and M. Malac, *App. Phys. Lett.*, 2009, **94**, 011915.

(18) M. Lazzeri, A. Vittadini and A. Selloni, *Phys. Rev. B*, 2001, **63**, 155409.

(19) H. G. Yang, C. H. Sun, S. Z. Qiao, J. Zou, G. Liu, S. Campbell Smith, H. M. Cheng and G. Q. Lu, *Nature*, 2008**, 453**, 638.

(20) X. H. Yang, Z. Li, G. Liu, J. Xing, C. Sun, H. G. Yang and C. Li, *CrystEngComm.*, 2011, **13**, 1378.

(21) W. Yang, J. Li, Y. Wang, F. Zhu, W. Shi, F. Wan and D. Xu, *Chem. Comm.*, 2011, **47**, 1809.

(22) C. Hsu, Y. Shen, Z. Wei, D. Liu and F. Liu, *J. Alloys Compd.*, 2014, **613**, 117.

(23) H. Dong, Z. Wu, Y. Gao, A. El-Shafei, S. Ning, J. Xi, B. Jiao and X. Hou, *Org. Electron.*, 2014**, 15**, 2847.

(24) H. Wang, T. You, W. Shi, J. Li and L. Guo, *J. Phys. Chem. C*, 2012, **116**, 6490.

(25) E. Fermi, *Phys. Rev.*, 1940, **57**, 485.

(26) R. Menzel, A. Duerrbeck, E. Liberti, H. C. Yau, D. W. McComb and M. S. P. Shaffer, *Chem. Mater.*, 2013, **25**, 2137.

(27) M. Stöger-Pollach, *Micron*, 2008, **39**, 1092.

(28) E. *Z.* Kröger, *Phys.*, 1968, **216**, 115.

(29) C. H. Chen and J. Silcox, *Solid State Comm.*, 1975, **17**, 273.

(30) S. C. Liou, M. -W. Chu, Y. J. Lee, M. Hong, J. Kwo and C. H. Chen, *New J. Phys.*, 2009, **11**, 103009.

(31) C. -T. Wu, M. -W. Chu, L. -C. Chen, K. -H. Chen, C. -W. Chen and C. H. Chen, *Micron*, 2010, **41**, 827.

(32) M. R. S. Huang, R. Erni, H. -Y. Lin, R. -C. Wang and C. -P. Liu, *Phys. Rev. B*, 2011, **84**, 155203.

(33) C. -T. Wu, M. -W. Chu, C. -P. Liu, K. -H. Chen, L. -C. Chen, C. -W. Chen and C. -H. Chen, *Plasmonics*, 2012, **7**,123.

(34) R. H. Ritchie, *Phys. Rev.*, 1957, **106**, 874.

(35) H. Raether, *Excitations of Plasmons and Interband Transitions by Electrons*, Springer Tracts in Modern Physics, New York, 1980.

(36) R. B. Pettit, J. Silcox and R. Vincent, *Phys. Rev B*, 1975, **11**, 3116.

(37) J. Nelayah, M. Kociak, O. Stéphan, N. Geuquet, L. Henrard, F. J. García de Abajo, I. Pastoriza-Santos, L. M. Liz-Marzan and C. Colliex, *Nano Lett.*, 2010, **10**, 902.

(38) J. Aizpurua, A. Howie and F. J. García de Abajo, *Phys. Rev. B*, 1999, **60**, 11149.

(39) R. Arenal, O. Stéphan, M. Kociak, D. Taverna, A. Loiseau and C. Colliex, *Microsc. Microanal.*, 2008, **14**, 274.

(40) M. Kociak, O. Stéphan, L. Henrard, V. Charbois, A. Rothschild, R. Tenne and C. Colliex, *Phys. Rev. Lett.*, 2001, **87**, 075501.

(40a) J. Nelayah, M. Kociak, O. Stéphan, F. J. García de Abajo, M. Tencé, L. Henrard, D. Taverna, I. Pastoriza-Santos, L. M. Liz-Marzán and C. Colliex, Nat. Phys., 2007, **3**, 348.

(40b) J. Nelayah, M. Kociak, O. Stéphan, N. Geuquet, L. Henrard, F. J. García de Abajo, I. Pastoriza-Santos, L. M. Liz-Marzán and C. Colliex, Nano Lett., 2010, **10**, 902.

(43) J. P. R. Bolton and M. Chen, *J. Phys. Condens. Matter*, 1995, **7**, 3405.

(44) T. Neyer, P. Schattschneider, J. P. R. Bolton and G. A. Botton, *J. Microsc.*, 1997, **187**, 184.

(45) R. O. Da Silva, R. H. Gonçalves, D. G. Stroppa; A. J. Ramirez and E. R. Leite, *Nanoscale,* 2011, **3**, 1910.

(46) C. M. McGilvery, A. E. Goodge, M. S. P. Shaffer and D. W. McComb, *Micron*, 2012, **43**, 450.